

Breast Cancer Diagnostics Using Angular View Infrared Images

Sabyasachi Samantaray^{a,1}, Kartik S. Nair^{a,2}, Matheus de Freitas Oliveira Baffa^{b,3}, and Thomas M. Deserno^{c,4}

^aIndian Institute of Technology Bombay, Department of Computer Science & Engineering, Mumbai, India

^bUniversity of São Paulo, Department of Computing and Mathematics, Ribeirão Preto, Brazil

^cPeter L. Reichertz Institute for Medical Informatics of TU Braunschweig & Hannover Medical School, Braunschweig, Germany

ABSTRACT

Worldwide, breast cancer presents a significant health challenge, necessitating innovative techniques for early detection and prognosis. Although mammography is the established screening method, it has drawbacks, including radiation exposure and high costs. Recent studies have explored the application of machine learning to frontal infrared images for breast cancer detection. However, the potential of infrared imaging from angular views has not been thoroughly explored. In this paper, we investigate, develop, and evaluate classification models for breast cancer diagnosis using lateral and oblique infrared images. Our approach incorporates radiomic features and Convolutional Neural Networks along with various feature fusion techniques to train deep neural networks. The primary objective is to determine the suitability of angular views for breast cancer detection, identify the most effective view, and assess its impact on classification accuracy. Utilizing the publicly available Database for Mammology Research with Infrared Images (DMR-IR), we apply an image processing pipeline for image improvement and segmentation. Additionally, we extract features using two strategies: radiomic features and convolutional neural network features. Subsequently, we conduct a series of k-fold cross-validation experiments to determine whether the features and feature fusion techniques are effective. Our findings indicate that oblique images, particularly when combined with DenseNet features, demonstrate superior performance. We achieved an average accuracy of 97.74%, specificity of 95.25%, and an F1 score of 98.24%. This study contributes to the advancement of machine learning in early breast cancer detection and underscores the significant potential of angular views in thermal infrared imaging, leading to improved diagnostic outcomes for patients worldwide.

Keywords: Breast Cancer, Convolutional Neural Network, Multi-View Classification, Thermography, Radiomic Features

1. INTRODUCTION

Breast cancer is a significant global health challenge that impacts millions of people worldwide. It is the most common cancer among women globally impacting low- and high-income countries.¹ According to the World Health Organization (WHO), breast cancer is the leading cause of cancer-related deaths among women worldwide.²

According to WHO statistics,² the global impact of breast cancer remains significant. In that year, there were 2.3 million women diagnosed with this disease, and it led to 685,000 deaths worldwide, which illustrates the need for effective detection and treatment strategies. Also, by the end of 2020, the number of women who had been diagnosed with breast cancer in the previous five years reached 7.8 million, making breast cancer the most prevalent cancer globally.

¹ Sabyasachi Samantaray, sachiray@cse.iitb.ac.in

² Kartik S. Nair, kartikn@cse.iitb.ac.in

³ Matheus F. O. Baffa, mbaffa@usp.br

⁴ Thomas Deserno, thomas.deserno@plri.de

Mammography is the most common screening device for breast cancer diagnosis. It is particularly effective in women over the age of 50, with an overall sensitivity of about 87 percent.³ However, its effectiveness may vary, especially in younger women with denser breast tissue, where false-negative results can occur. To address these limitations, researchers explore innovative techniques, such as machine learning algorithms applied to a variety of imaging modalities.

Infrared imaging, specifically thermography, has emerged as a promising tool for early cancer detection. The temperature distribution in healthy individuals tends to exhibit symmetry over the sagittal axis and remains consistent over time. In cancerous tissues, there may be asymmetries attributed to increased blood flow and metabolic changes.⁴ This difference in thermal patterns presents an opportunity for thermography to be utilized for early detection of breast cancer.

Numerous studies have focused on frontal view imaging for breast cancer detection, demonstrating good accuracy and sensitivity.^{5,6} However, lateral and oblique views have a high diagnostic value.⁷ There is a notable gap for infrared imaging that specifically concentrates on using only side views without incorporating frontal and clinical data.

Angular images offer a unique perspective of breast tissue, which may not be as effectively captured in frontal views. These side views can potentially reveal subtler thermal anomalies and vascular patterns that are indicative of early-stage breast cancer, which might be obscured in frontal imaging due to overlapping tissues or varying breast densities. Moreover, lateral views are particularly beneficial in visualizing the outer quadrants of the breast, where a significant proportion of breast cancer develops.

The purpose of this study is to conduct a comprehensive analysis of lateral and oblique images for breast cancer detection. By evaluating the individual impact of lateral and oblique images without the use of other information, such as frontal features or clinical data, our research aims to determine if angular images alone can suffice for the accurate diagnosis of breast cancer.

2. RELATED PAPERS

In the field of breast cancer detection, much of the existing research focuses on the frontal view imaging. This area has been extensively studied, leading to a wealth of knowledge and improved methods in detecting breast cancer from frontal images. However, the study of angular view imaging is much less common. The use of angular views in breast cancer imaging is an area that has not been thoroughly investigated, creating a gap in the research. This section will describe the current state-of-the-art in the detection of breast cancer in the lateral and oblique view.

Madhavi and Thomas⁸ developed a method for breast infrared image analysis using multi-view textural feature fusion. Their technique involved extracting textural features from the images, utilizing methods like the grey-level co-occurrence matrix, grey-level run length matrix, grey-level size zone matrix, and the neighbourhood grey tone difference matrix. These methods are designed to quantitatively analyze local and regional textures in the images. Their dataset comprised approximately 63 images, split between 32 normal and 31 abnormal cases. The proposed method demonstrated high accuracy in its results, achieving an overall accuracy rate of 96%, 100% sensitivity rate, and a specificity of 92%.

In 2021, Sánchez-Cause *et al.*⁹ developed a classification method for multi-view infrared images. Their method involved using both frontal and side views as inputs in a CNN. This approach combined features from the different views within the CNN, resulting in a unified prediction. The method achieved an overall accuracy of 97%, with a sensitivity of 83% and a specificity of 100%.

Mammootttil *et al.*¹⁰ proposed a comprehensive classification method that incorporates a multi-angle approach, including angular and frontal views, in conjunction with clinical data like age and symptoms. Their method utilized a CNN for the spatial analysis of images, which was then integrated with clinical data processed through a separate neural network. This approach, combining diverse image angles with relevant clinical information, yielded an accuracy of 93.8%, with a specificity of 96.7% and a sensitivity of 88.9%.

Ensafi *et al.*¹¹ conducted an evaluation of several pretrained deep learning models for detecting breast cancer in infrared images. They tested models including VGG16, VGG19, EfficientNetB0, Resnet50, DenseNet121,

and DenseNet201, applying them to images captured from multiple views such as angular and frontal. The DenseNet201 model demonstrated the best performance in their study, achieving an accuracy of 93%, along with a sensitivity and specificity of 93% and 95%, respectively.

Pramanik *et al.*¹² developed a new method for detecting breast cancer using side view infrared images. Their approach focuses on creating two specific types of feature images: magnitude features of breast thermogram (MFBT) and orientation features of breast thermogram (OFBT). These images are processed to produce a 36-element feature vector, which forms the basis for training a feed-forward artificial neural network. The network operated on a gradient descent training rule. The authors reported that this method was highly effective, achieving a classification accuracy of 98.6%. It demonstrated a sensitivity of 100% and a specificity of 97.8%.

2.1 Our Contributions

The majority of existing literature predominantly focuses on the combined use of angular and frontal views in breast cancer detection, a method previously established as effective. However, there remains a significant gap in understanding the standalone efficacy of the lateral and oblique view. Furthermore, conventional approaches in this domain often rely on CNN or textural features for classification. Our paper makes key contributions in this context:

- A comprehensive analysis of the effectiveness of using only the angular view in breast cancer detection, exploring its impact on classification accuracy.
- The development of a novel classification technique that leverages radiomic features, providing a new perspective in breast cancer detection methodologies.
- The development of an advanced classification approach using CNN and radiomic features, aiming to enhance diagnostic precision and reliability.

3. MATERIALS AND METHODS

We developed a methodical approach that encompasses a series of steps designed to preprocess images, extract features, and utilized these features for training a classification algorithm (Figure 1). The process begins with the input of angular images into our preprocessing algorithm. This algorithm is responsible for converting colored images into grayscale and implementing the BM3D denoising technique to enhance image quality.

Subsequently, we employed a U-Net CNN to precisely segment the region of interest. This step ensures the exclusion of irrelevant elements such as background clutter and abdominal regions, focusing solely on the areas pertinent to breast cancer detection.

The feature extraction phase of our method involves two distinct strategies. The first strategy is centered around the extraction of radiomic features, coupled with the evaluation of various fusion techniques applied across all four angles. The second strategy delves into feature extraction using a DenseNet CNN. Similar to the first strategy, this also involves generating and evaluating features for all four image angles, with different feature fusion techniques.

We evaluate our classification model across all possible combinations of feature extraction and fusion techniques. The culmination of this process is the identification and reporting of the most effective combination, ensuring optimal accuracy and reliability in breast cancer detection through our proposed method. In this section, we discuss each of these steps in depth.

3.1 Dataset Description

This paper utilizes infrared images from the publicly available database for mastology research with infrared images (DMR-IR).¹³ The DMR-IR repository contains infrared images obtained through both dynamic and static protocols. The dynamic approach involves capturing a series of 20 frontal images at regular intervals following body cooling to a specific temperature. In contrast, the static method captures single images from distinct angles once thermal stability is reached. The static protocol produces a total of five images, comprising one frontal view (at 0°, two oblique images (at right 45° and left 45°), and two lateral images (at right 90° and

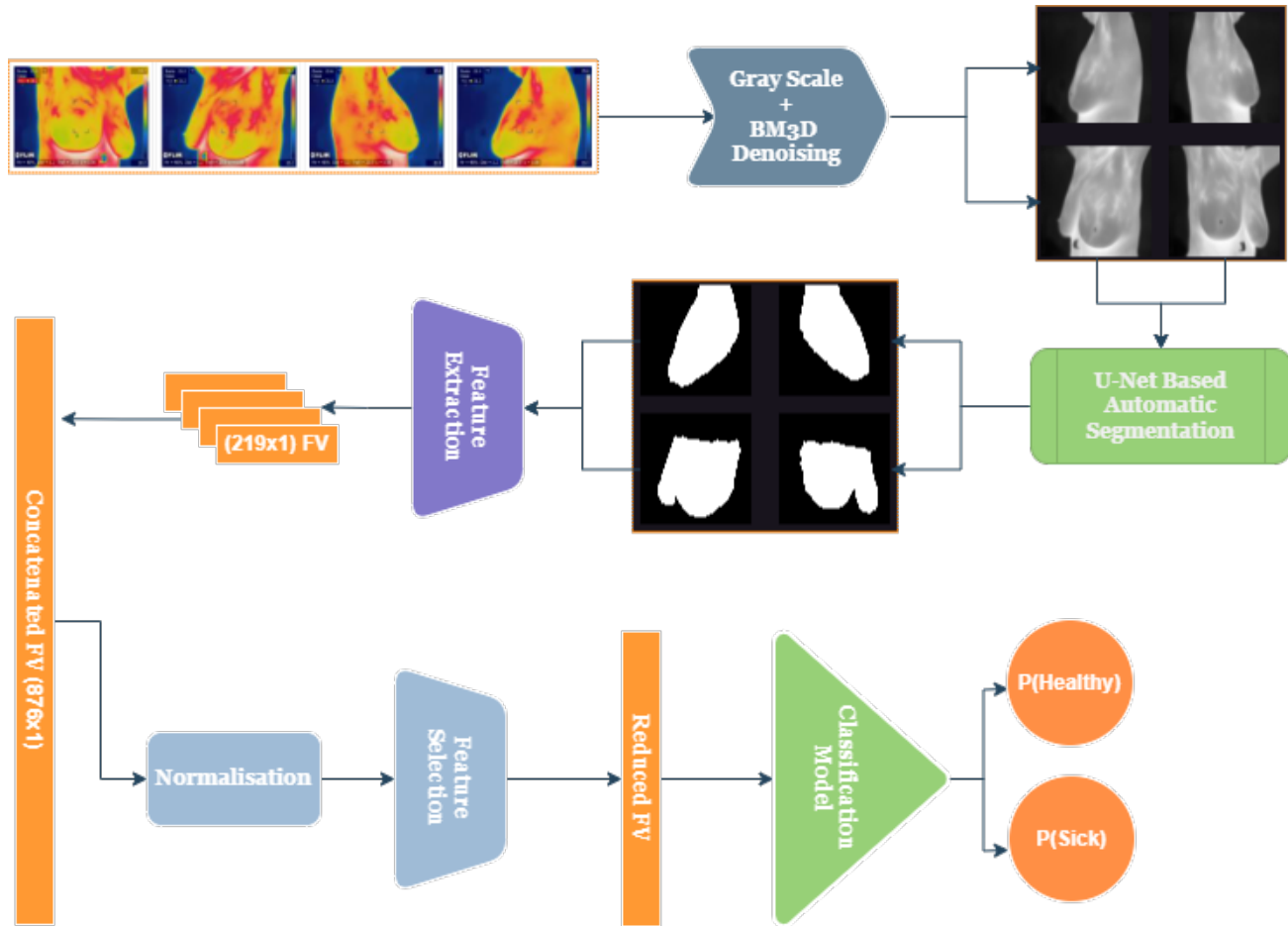


Figure 1. The workflow of infrared preprocessing and information flow.

left 90°). Given our focus on side view performance, we specifically utilized lateral and oblique images from the static protocol (Table I). We cleaned the dataset by removing samples with unknown diagnoses, patients with missing thermal matrices or angles, extremely blurry images, incorrect labels, those not adhering to the acquisition protocol, and duplicated images.

Table 1. Distribution of healthy/sick patients after data cleansing for each of the multi-view combinations.

Views	Total Patients	Healthy Patients	Sick Patients
Oblique Views (R_45 and L_45)	264	152	112
Lateral Views (R_90 and L_90)	283	168	115
All Angular Views (R_90,R_45,L_45,L_90)	256	149	107

3.2 Image Preprocessing

In the DMR-IR dataset, images vary between color-coded and grayscale formats. To achieve uniformity, we implemented a matrix-to-image conversion that normalizes image data within a 0 to 255 range. For image enhancement, we applied two techniques: block matching 3D filtering (BM3D) for denoising and contrast limiting adaptive histogram equalization (CLAHE) method to improve contrast (Figure 2). BM3D is denoising method which employs block matching and collaborative filtering for effective noise removal. We used the `bm3d.bm3d` function with `sigma_psd=0.2`, which estimates the noise standard deviation, where a lower value is indicative of enhanced noise reduction. To ensure thorough noise elimination while maintaining image detail, we utilized all stages of the BM3D pipeline.¹⁴

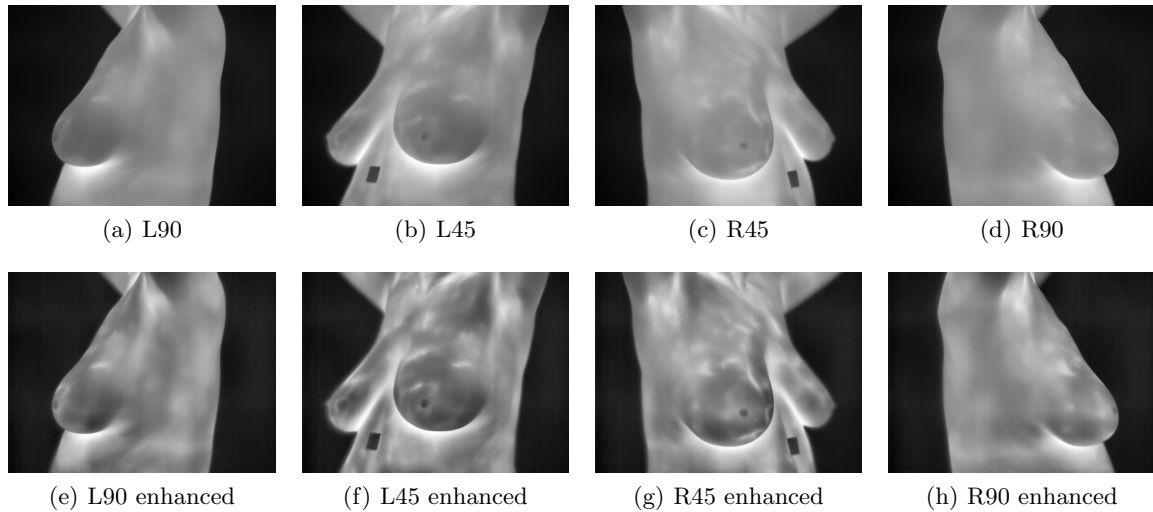


Figure 2. Images before and after image preprocessing for patient ID 222 of the DMR-IR Database belonging to the healthy category.

To enhance the dataset, we focused on segmenting the region of interest (ROI) to accurately extract key anatomical features, thereby improving the accuracy of our analyses (Figure 3). For segmentation, we adapted a U-Net based method originally developed by Carvalho *et al.*¹⁵ While the original model used a 64×64 input size for angular images, we found this insufficient for our needs. Consequently, we employed a modified U-Net model with an increased input size of 256×256 , allowing for more detailed extraction of segmentation masks.

Our customized U-Net comprises 18 convolutional layers, each followed by batch normalization. The architecture is divided into two segments: the first 10 layers are dedicated to down-sampling, utilizing max pooling with a 2×2 window size. The subsequent layers focus on up-sampling, also employing a 2×2 window size. We used the rectifier linear unit (ReLU) as the activation function. During the down-sampling phase, the convolutional layers were configured to extract filters in a hierarchical manner: starting with 256 filters, then reducing to 128, 64, 32, and finally 16 filters.

Similarly, during up-sampling, we extract 16, 32, 64, 128, and 256 filters. All filters have a size of 3×3 . Finally, the output layer consists of a single convolutional layer with a 1×1 size, using the Sigmoid activation function. We trained this architecture using the Adam optimizer with a learning rate of $1e-3$ and employed the Sørensen-Dice Loss function. To avoid overfitting, an early stopping mechanism was implemented, which halts training if the validation loss does not improve for 10 consecutive epochs. Despite the limited availability of a gold standard for angular images, our model achieved segmentation masks with an Intersection over Union (IoU) of 85.43%, accuracy of 92.91%, and a Dice Score of 91.97%.

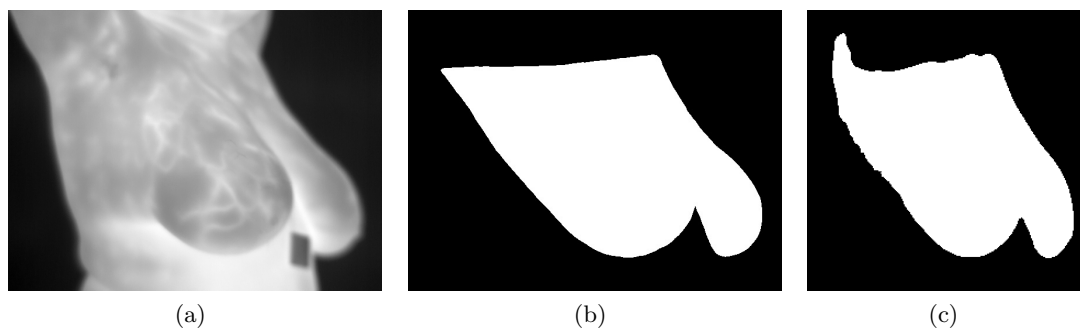


Figure 3. (From left to right) a. Original grayscale lateral right 45° image of patient ID 31 (Healthy) from the DMR Database; b. corresponding gold standard segmentation mask; c. segmentation result using U-Net.

3.3 Feature Extraction Strategies

We evaluated two distinct classification strategies using all four side views: (i) feature extraction and fusion, and (ii) pre-trained convolutional neural networks (CNNs). The first strategy extracts and combines radiomic features from the side views to form a unified representation. In total, we extracted 93 radiomic features using the PyRadiomics Framework,¹⁶ which comprises the following features: 18 first-order statistics, 24 gray level co-occurrence matrix, 16 gray level run length matrix, 16 gray level size zone matrix, five neighboring gray tone difference matrix, and 14 gray level dependence matrix. We also extract 126 features using the Mahotas Framework,¹⁷ in particular 36 local binary patterns, 36 Zernike moments, and 54 threshold adjacency statistics. For each angular image, the final feature vector has 219 entries.

The second strategy encompasses a DenseNet CNN to extract features from each side. We first fine-tuned the pretrained CNN model using infrared images. Then, we extracted the CNN's feature maps for each side view image using the second last available convolutional layer of the DenseNet architecture. This approach generates 1024 features per image.

After extracting the features using the strategies, we combined the image angles using different fusion techniques: sum, product, concatenation, and max. This fusion strategy enabled us to explore various combinations of the features, allowing the models to capture more complex patterns and relationships within the data.

Finally, we used analysis of variance (ANOVA) to select the best features, identifying those that most effectively differentiate between cancerous and non-cancerous thermal images. This selection process streamlined the dataset, focusing on essential characteristics, and paved the way for more accurate and efficient classification in our deep neural network models for breast cancer detection.

3.4 Classification Methodology

The classification methodology uses a fully-connected neural network (FCNN). The network consists of 86 hidden layers, each containing five neurons, followed by an output layer with two neurons. Within the hidden layers, the rectified linear unit (ReLU) activation function is applied to introduce non-linearity and enable the network to capture complex relationships within the data. In the output layer, we use the softmax activation function to produce probability distributions for the binary classification task. Besides, we used the Adam optimizer with the default learning rate and the binary cross-entropy loss function. We set the maximum number of training epochs to 1,000, but due to the early stopping criterion, our training typically concludes around 250 epochs. This helps to prevent over-fitting and ensures efficient training. We set the batch size to 32, balancing computational efficiency and gradient estimation accuracy.

For strategy two, we utilized two FCNN architectures, one for concatenated features and one for the other fusion techniques. The FCNN for concatenated features requires a different architecture since its input size is larger. To concatenate all four side images, we compose a FCNN of eight layers. The first layer had 4096 neurons, responsible for receiving the 1024 features from each side image. The six hidden layers had 2048, 1024, 1024, 256, 128, and 64 neurons using the ReLU activation function. A dropout layer follows each hidden layer, randomly turning off 20% of the neurons. The output layer with two neurons represents the two classes and uses the softmax activation function.

The FCNN architecture for the other fusion techniques had seven layers. The input layer receives the 1024 features obtained after the fusion of each side. Further, we have five hidden layers, with 512, 256, 128, 64, and 64 neurons using the ReLU activation function. Similar to the concatenated approach, we use dropout layers and a binary output layer with the softmax activation function for binary classification. We designed these architectures empirically to optimize the classification performance.

4. EXPERIMENTAL DESIGN

To make the experiments and develop this research, we utilized a Linux Ubuntu server equipped with two Intel Xeon Silver processors, 192 GB of DDR4 RAM, and two NVIDIA RTX A4000 graphics cards. The development used Python 3.10, with OpenCV 4 and Tensorflow 2.10.

In our experiments, we used the k-fold cross-validation protocol, with $k = 10$. This protocol divides the dataset into ten parts. In each iteration, nine parts are used for training the model and one part for testing. This procedure is repeated ten times, with each part being used once as the test set.

To ensure the validity of the validation process, patient data were carefully separated to prevent any overlap between training and testing datasets across all iterations. This method ensures unbiased evaluation and generalizability of the model’s performance.

To quantitatively evaluate our method’s efficiency, we utilized five metrics: accuracy, precision, recall, specificity, and area under the curve (AUC). Accuracy measures the overall correctness of the model by calculating the proportion of true positives and true negatives. Precision assesses the ratio of true positives among all positive predictions, while recall, or sensitivity, evaluates the model’s ability to correctly identify actual positives. Specificity focuses on correctly identifying true negatives, ensuring the model’s precision in negative case detection. Lastly, the AUC, derived from the ROC curve, provides an aggregate measure of performance across various thresholds, with higher values indicating better diagnostic accuracy.

5. RESULTS

In our study, we conducted a series of experiments with the radiomics and mahotas features to assess the performance of our classification model (Table 2). These experiments were categorized based on the type of image used: lateral images, oblique images, and a combination of all angular images. For each category, we employed different feature selection and fusion techniques, namely no feature selection (No FS) with concatenation, and ANOVA. The performance of each experiment was evaluated using several metrics, including accuracy, precision, recall, specificity, and AUC. The results demonstrated that the combination of all angular images with NoFS and sum fusion yielded the highest accuracy, precision, and AUC, indicating its effectiveness in the classification task. Conversely, the experiments with lateral and oblique images showed slightly lower performance metrics, yet provided valuable insights into the specific advantages of each imaging perspective and feature fusion technique.

Table 2. Experiments with radiomics and mahotas features.

Experiment	FS and Fusion	Accuracy	Precision	Recall	Specificity	AUC
Lateral Images	No FS and Concat	87.30%	90.57%	87.96%	85.51%	91.58%
Oblique Images	ANOVA and Sum	85.17%	86.06%	89.08%	79.05%	90.31%
All Angular	No FS and Sum	90.21%	93.01%	89.63%	90.28%	92.60%

The DenseNet features extracted from all four side images, combined with ANOVA feature selection and the sum fusion technique, achieved the highest performance (Table 3). The average accuracy, sensitivity, and AUC is 97.74%, 98.61%, and 99.17%, respectively. Hence, the second strategy is the most effective for the proposed problem in contrast to the best configuration for the first strategy.

Table 3. Experiments with DenseNet features.

Experiment	FS and Fusion	Accuracy	Precision	Recall	Specificity	AUC
Lateral Images	ANOVA and Concat	95.38%	95.43%	97.15%	95.45%	98.64%
Oblique Images	ANOVA and Sum	97.73%	98.01%	98.60%	95.25%	99.17%
All Angular	ANOVA and Concat	97.69%	97.57%	98.75%	96.18%	98.60%

To deeply describe the results of the second strategy, Table 4 presents the per-fold outcomes for our DenseNet-based approach. The model demonstrates good consistency and effectiveness across all evaluation metrics. In eight out of ten folds, it achieved a score of 100% in terms of accuracy, precision, recall, specificity, F1-score, and AUC. The two remaining folds, while not attaining the 100% mark, still exhibited strong performances with accuracies of 92.31% and 88.89%, and AUCs of 95.63% and 96.05%, respectively. The mean values across all folds—97.74% for accuracy, 98.61% for sensitivity, and 99.17% for AUC—further underscore the robustness and reliability of our model in processing oblique images. Additionally, the low standard deviation values highlight the model’s consistent performance across different subsets of data.

Table 4. Detailed K-Fold cross validation results for our best performing experiment on oblique images using strategy 2.

Fold	Accuracy	Precision	Recall	Specificity	F1-Score	AUC
0	100.0%	100.0%	100.0%	100.0%	100.0%	100.0%
1	88.89%	86.36%	100.0%	62.5%	92.68%	96.05%
2	100.0%	100.0%	100.0%	100.0%	100.0%	100.0%
3	100.0%	100.0%	100.0%	100.0%	100.0%	100.0%
4	96.15%	100.0%	92.31%	100.0%	96.0%	100.0%
5	100.0%	100.0%	100.0%	100.0%	100.0%	100.0%
6	100.0%	100.0%	100.0%	100.0%	100.0%	100.0%
7	100.0%	100.0%	100.0%	100.0%	100.0%	100.0%
8	92.31%	93.75%	93.75%	90.0%	93.75%	95.63%
9	100.0%	100.0%	100.0%	100.0%	100.0%	100.0%
Mean	97.74%	98.01%	98.61%	95.25%	98.24%	99.17%
Std. Dev.	±3.82	±4.31	±2.81	±11.32	±2.79	±1.67

6. DISCUSSION

While the method presents significant advantages, there are also some limitations that must be acknowledged. The method’s reliance on lateral and oblique images represents both a strength and a challenge. While the angular views enhance accuracy in breast cancer detection, their utilization may necessitate specific expertise in imaging. Unlike traditional imaging approaches, lateral and oblique views require specialized calibration and alignment processes that may not be readily available in all medical settings. This potentially limits the accessibility.

However, angular images offer distinct advantages to clinicians. They provide a different perspective that may reveal details not visible in frontal views, therefore enhancing the diagnostic process. By implementing various angles and views, clinicians can gain a more comprehensive understanding of the underlying pathology. This additional information can complement the frontal diagnosis, revealing aspects that might be obscured or overlooked from a frontal view alone. Therefore, the integration of angular images, despite initial challenges, could be a vital step toward more accurate and personalized breast cancer detection.

Given that oblique images achieve a 97.74% accuracy rate, they indeed hold significant potential for detecting breast cancer. While this is slightly lower than the 98% accuracy achieved by frontal images alone,¹⁸ it’s still a high level of accuracy and suggests that angular images can be quite effective in identifying breast cancer. Still, the true potential lies in the combined use of both angular and frontal images. When used together, they can provide a more comprehensive analysis, potentially leading to even higher accuracy and reliability in diagnosis. The complementary perspectives offered by both types of images can enhance the detection of tumors that might be less visible in one view but more apparent in another.

For future work, we intend to reduce the method’s complexity by implementing state-of-the-art algorithms, such as transformers, and evaluate other approaches, such as 3D CNNs.

7. CONCLUSION

This study delved into the potential of lateral and oblique thermal images for breast cancer detection, specifically exploring their diagnostic effectiveness when used in isolation. Throughout our experiments we detected that Oblique images with DenseNet features are the best angle for imaging besides frontal. Leveraging the DMR-IR database, a specifically designed preprocessing pipeline, and a deep neural network approach, our findings highlight the value of these views, thereby contributing to the evolution of breast cancer detection techniques.

Acknowledgment

M.F.O.B. is supported in part by Coordination for the Improvement of Higher Education Personnel (CAPES) under grant 88887.498626/2020-00 and 88887.695355/2022-00.

REFERENCES

- [1] Bray, F., Ferlay, J., Soerjomataram, I., Siegel, R. L., Torre, L. A., and Jemal, A., “Global cancer statistics 2018: Globocan estimates of incidence and mortality worldwide for 36 cancers in 185 countries,” *CA: a cancer journal for clinicians* **68**(6), 394–424 (2018).
- [2] World Health Organization, “Breast cancer.” <https://www.who.int/news-room/fact-sheets/detail/breast-cancer> (2023). Accessed: 2024-01-25.
- [3] Lehman, C. D., Arao, R. F., Sprague, B. L., Lee, J. M., Buist, D. S., Kerlikowske, K., Henderson, L. M., Onega, T., Tosteson, A. N., Rauscher, G. H., and Miglioretti, D. L., “National performance benchmarks for modern screening digital mammography: Update from the breast cancer surveillance consortium,” *Radiology* **283**(1), 49–58 (2017).
- [4] Amalu, W., Hobbins, W., Head, J., and Elliot, R., “Infrared imaging of the breast—an overview,” *The Biomedical Engineering Handbook, 3rd ed., Medical Devices and Systems*. CRC Press, Baton Rouge (2006).
- [5] Baffa, M. d. F. O. and Conci, A., “Radiomics for breast ir-imaging classification,” in [*MICCAI Workshop on Medical Image Assisted Biomarkers’ Discovery*], 10–19, Springer (2022).
- [6] Resmini, R., da Silva, L. F., Medeiros, P. R., Araujo, A. S., Muchaluat-Saade, D. C., and Conci, A., “A hybrid methodology for breast screening and cancer diagnosis using thermography,” *Computers in Biology and Medicine* **135**, 104553 (2021).
- [7] Lundgren, B., “The oblique view at mammography,” *The British journal of radiology* **50**(597), 626–628 (1977).
- [8] Madhavi, V. and Thomas, C. B., “Multi-view breast thermogram analysis by fusing texture features,” *Quantitative InfraRed Thermography Journal* **16**(1), 111–128 (2019).
- [9] Sánchez-Cauce, R., Pérez-Martín, J., and Luque, M., “Multi-input convolutional neural network for breast cancer detection using thermal images and clinical data,” *Computer Methods and Programs in Biomedicine* **204**, 106045 (2021).
- [10] Mammoottil, M. J., Kulangara, L. J., Cherian, A. S., Mohandas, P., Hasikin, K., Mahmud, M., et al., “Detection of breast cancer from five-view thermal images using convolutional neural networks,” *Journal of Healthcare Engineering* **2022** (2022).
- [11] Ensafi, M., Keyvanpour, M. R., and Shojaedini, S. V., “A new method for promote the performance of deep learning paradigm in diagnosing breast cancer: improving role of fusing multiple views of thermography images,” *Health and Technology* **12**(6), 1097–1107 (2022).
- [12] Pramanik, S., Bhattacharjee, D., and Nasipuri, M., “Multi-resolution analysis to differentiate the healthy and unhealthy breast using breast thermogram,” in [*2016 international conference on systems in medicine and biology (ICSMB)*], 49–52, IEEE (2016).
- [13] da Silva, L. F., Saade, D. C. M., Sequeiros, G. O., Silva, A. C., de Paiva, A. C., de Souza Bravo, R., and Conci, A., “A new database for breast research with infrared image,” *Journal of Medical Imaging and Health Informatics* **4**, 92–100 (2014).
- [14] Sriraam, N., Kavya, N., Usha, N., D, S., Balasubramaniam, V., and Menaka, M., [*Quantitative Analysis of Breast Thermograms Using BM3D Denoising Method and Features Extraction*], 781–793 (01 2022).
- [15] de Carvalho, E. C., Coelho, A. M., Conci, A., and de Freitas Oliveira Baffa, M., “U-net convolutional neural networks for breast ir imaging segmentation on frontal and lateral view,” *Computer Methods in Biomechanics and Biomedical Engineering: Imaging & Visualization* **11**(3), 311–316 (2023).
- [16] Van Griethuysen, J. J., Fedorov, A., Parmar, C., Hosny, A., Aucoin, N., Narayan, V., Beets-Tan, R. G., Fillion-Robin, J.-C., Pieper, S., and Aerts, H. J., “Computational radiomics system to decode the radiographic phenotype,” *Cancer research* **77**(21), e104–e107 (2017).
- [17] Coelho, L. P., “Mahotas: Open source software for scriptable computer vision,” *arXiv preprint arXiv:1211.4907* (2012).
- [18] Baffa, M. d. F. O. and Lattari, L. G., “Convolutional neural networks for static and dynamic breast infrared imaging classification,” in [*2018 31st SIBGRAPI Conference on Graphics, Patterns and Images (SIBGRAPI)*], 174–181, IEEE (2018).